

NUMERICAL INVESTIGATION ON THE INFLUENCE OF ANISOTROPIC SURFACE STRUCTURES ON THE SKIN FRICTION

S. Hohenstein - J. Seume

Institute of Turbomachinery and Fluid Dynamics
Leibniz Universität Hannover, Appelstr. 9, 30165 Hannover, Germany
Hohenstein@tfd.uni-hannover.de

ABSTRACT

The present study investigates the effect of anisotropic surface roughness on flow losses using Large-Eddy-Simulation (LES) and compares the results to a model based on the equivalent sand grain roughness. For this comparison models of surface roughness are built from measurements of real roughness to isolate the effect of anisotropy for which two orthogonal main flow directions with respect to the anisotropy of the surface are investigated. For these two directions an equivalent sand grain roughness height is calculated using the roughness element shape and density parameter. The shift of the velocity distribution is then predicted by using a roughness function and compared with the results of the LES. Furthermore, the rough and smooth-wall velocity distributions are compared with each other in velocity defect form to check the Reynolds number similarity hypothesis. Both comparisons show a good agreement thus confirming with LES that the simple model of equivalent sand grain roughness is an appropriate method to predict the influence of anisotropic surface roughness on skin friction.

NOMENCLATURE

A_s	frontal surface area	\bar{S}_{ij}	Shear strain tensor
A_f	windward wetted surface	u_b	bulk velocity
B'_{FR}	Nikuradse roughness function	u_e^+	boundary layer edge velocity
C^+	integration constant	u_τ	friction velocity
C_s	Smagorinsky constant	u^+	dimensionless velocity
h	local roughness height	Δu^+	roughness function
k	roughness height	y^+	dimensionless wall distance
k_s	equivalent sand grain height	<i>Greek symbols</i>	
l	local roughness length	δ	boundary layer thickness
N	number of nodes	δ	channel half height
Ra	arithmetic averaged roughness height	Δ	filter width
Re	Reynolds number	ν	kinematic viscosity
Re_τ	friction velocity Reynolds number	κ	von Kármán constant
Rz	averaged maximum roughness height	Λ_s	roughness element shape parameter
S	reference area	ρ	density
S_f	total frontal area	μ^{sgs}	sub-grid-scale viscosity
		τ_w	wall shear stress

INTRODUCTION

The effect of surface roughness on fluid flow has been first studied by Nikuradse (1933) and Schlichting (1936) with the result that surface roughness, especially in turbulent boundary layers,

leads to a significant increase in losses. Nikuradse investigated the pressure loss of sand roughened pipe walls and introduced the dimensionless roughness parameter $k_s^+ = k_s u_\tau / \nu$ to describe the roughness. Later on Schlichting used the data of Nikuradse to describe other types than sand grain roughness. He introduced a standard roughness height k_s to describe the effects of any roughness type onto the fluid flow. The standard roughness assumes that the roughness of a surface is composed of spheres placed on the surface in the most dense arrangement, as shown in Fig. 1. Since this arrangement is typical for sand paper, the standard roughness height is also called sand grain roughness height. For engineering applications any technical roughness height can be described in terms of an equivalent sand grain roughness height. To do so the skin friction of an arbitrary roughness is correlated to a sand grain roughness height with the same skin friction.

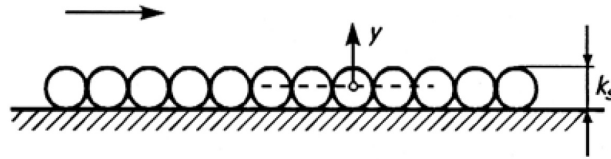


Figure 1: **Definition of standard roughness height, Schlichting and Gersten (2005)**

Extensive measurements on surface roughness relevant for turbomachinery applications have been carried out by Achary et al. (1986). They correlated the effect of surface roughness onto the boundary layer's velocity distribution to the arithmetic mean roughness height Ra of the surface roughness and proposed a correlation $k_s = 4.2Ra$ for a limited class rough surfaces. It has been shown in recent years that the model of equivalent sand grain roughness has its limitations. This is particularly true when the shape of the roughness is of a non-uniform, especially anisotropic type and when correlating roughness parameters such as Ra to k_s . The flow over anisotropic surface roughness was numerically investigated among others by Ikeda and Durbin (2007), Cui et al. (2003a) and Cui et al. (2003b). The latter ones used LES to investigate roughness made of ribs and sinusoidal waves under cross flow conditions in channel flows. Using the classical model of equivalent sand grain roughness, the influence of the ribs and waves is underestimated. For the rib roughness, the height of an equivalent sand grain roughness had to be six times higher and for the sinusoidal waves the equivalent sand grain height should be three times higher than predicted. Further numerical investigations considering the effect of surface roughness have been carried out by Singh et al. (2007) and Iacone et al. (2008) who built surface roughness using spheres and ribs.

Figure 2 shows the surface roughness topology of a high pressure turbine blade, which has no thermal barrier coating, in operating condition. It is obvious that real surface roughness is a combination of both isotropic and anisotropic roughness elements, and is much more complex than the cases mentioned above. Several correlations were developed in order to take this complexity into account. An overview is given by Sigal and Danberg (1990) who also proposed a new correlation to consider the shape and density of two-dimensional roughness elements with respect to the flow direction. Hence, a new equivalent sand grain height k_s can be calculated with the new parameter Λ_s , as introduced by Sigal and Danberg (1990).

The approach of Sigal and Danberg (1990) was picked up and modified by van Rij et al. (2002) to fit three-dimensional, irregular surface roughness, which was the subject of their investigation. The modified correlation works well for isotropic roughness. Further work on the characterization and prediction of the skin friction of real surface roughness was conducted by Bons et al. (2001), Bons (2002), Bons (2005), and Bons (2010), who also modified the correlations proposed by Sigal and Danberg (1990). A comprehensive overview of the different correlations to characterize surface roughness is given by Flack and Schultz (2010).

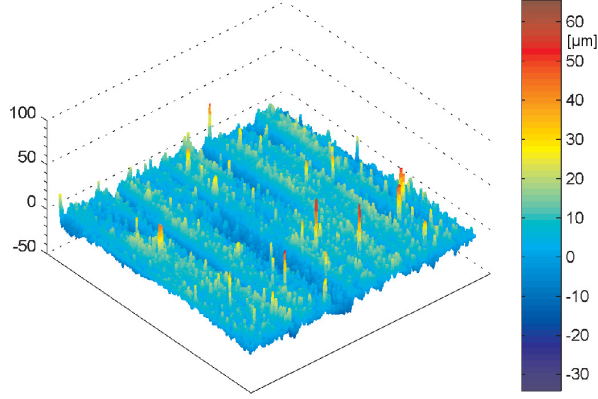


Figure 2: **Real turbine surface roughness**

The investigations carried out so far are of two types. On one hand, experimental investigations were carried out on real surface roughness. The big disadvantage of this method is that flow close to the wall and the roughness elements could not be resolved. On the other hand, there are numerical investigations using LES and Direct-Numerical-Simulations (DNS) which allow extending the investigation to the whole boundary layer flow down to the wall. These methods however are restricted to simple generic roughnesses, because spatial discretization is achieved with structured grids. In the present study, Large-Eddy-Simulations are carried out on a surface roughness model, which is more realistic than the roughnesses used in the previous studies of Cui et al. (2003a) and Cui et al. (2003b).

BACKGROUND

The boundary layer of turbulent flows can be divided into three parts. Near the wall, for $y^+ \leq 5$, with $y^+ = \frac{y \cdot u_\tau}{\nu}$, only laminar friction is present. This part is called the viscous sublayer and the velocity, presented in inner-scaling in Eq. 1, is linearly dependent on the wall distance

$$u^+ = y^+. \quad (1)$$

In the buffer layer ($5 < y^+ \leq 70$) both, laminar and turbulent, stresses exist. Various equations are used to describe the dependency of u^+ from y^+ which are formulated among others by Schlichting and Gersten (2005). For values of $y^+ > 70$, only turbulent stresses are present. The course of the velocity distribution is described by Eq. 2, the "log law"

$$u^+ = \frac{1}{\kappa} \cdot \ln \left(\frac{y \cdot u_\tau}{\nu} \right) + C^+ - \Delta u^+ \quad (2)$$

where κ is the von Kármán constant and C^+ an integration constant. The von Kármán constant is usually assumed to be $\kappa \approx 0.41$ which is a good assumption for laboratory experiments, but as shown by Frenzen and Vogel (1995) and Cai and Steyn (1996), the von Kármán constant can vary in the range of $0.3 \leq \kappa \leq 0.48$. Particularly Frenzen and Vogel (1995) showed that κ is strongly dependent on the wall roughness.

Surface roughness leads to a shift of the logarithmic velocity profile and is described by the last term on the right hand side of Eq. 2, Δu^+ , which is called "roughness function". Depending on the height of the roughness elements, surface roughness can be classified as hydraulically smooth for $k_s^+ \leq 5$, transitionally rough for $5 < k_s^+ \leq 70$ and fully rough for $k_s^+ > 70$ with

$$k_s^+ = \frac{k_s \cdot u_\tau}{\nu}. \quad (3)$$

To check the Reynolds number similarity hypothesis the "law of the wall" can also be rewritten in form of the velocity defect as

$$u_e^+ - u^+ = -\frac{1}{\kappa} \ln(\eta) + B_1 - \frac{\Pi}{\kappa} \omega(\eta) \quad (4)$$

with $\eta = y/\delta$, B_1 being defined as $2\Pi/\kappa$ and the wake function ω (Schultz and Flack (2007)). The Reynolds number similarity hypothesis "states that the turbulence beyond a few roughness heights from the wall is independent of the surface condition" (Flack et al., 2005, pg.1). This assumes that the height of the roughness k is very small compared to the boundary layer thickness δ .

For fully rough surfaces, the roughness function is defined by Schultz and Flack (2007) as

$$\Delta u^+ = \frac{1}{\kappa} \ln(k_s^+) + C^+ - B'_{FR}. \quad (5)$$

In Eq. 5 B'_{FR} is the Nikuradse roughness function which in the fully rough flow regime equals $B'_{FR} = 8.5$. The equivalent sand grain height can be calculated with a correlation of Bons (2005), given in Eq. 6.

$$\log\left(\frac{k_s}{k}\right) = -0.43 \log(\Lambda_s) + 0.82 \quad (6)$$

and made dimensionless in units of inner scaling with the friction velocity and the kinematic viscosity.

The roughness element shape and density parameter Λ_s , given in Eq. 6, was introduced by Sigal and Danberg (1990). It takes into account the reference area S without any roughness and the total frontal surface area of the roughness elements S_f . Furthermore the windward wetted surface area A_f and the frontal surface area A_s of a roughness element are taken into account.

$$\Lambda_s = \frac{S}{S_f} \left(\frac{A_f}{A_s}\right)^{-1.6} \quad (7)$$

Originally Λ_s was defined for two dimensional homogenous surface roughness. Bons (2005) modified the definition of the parameter to be applicable to real surface roughness. The definitions of Bons (2005), Eq. 6 and Eq. 8, are also used in the current study to calculate Λ_s and determine an equivalent sand grain roughness.

$$\Lambda_s = \frac{\sum dx_i}{\sum \Delta h_i} \left(\frac{\sum \Delta h_i}{\sum l_i}\right)^{-1.6} \quad (8)$$

COMPUTATIONAL SETUP

Numerical Method

The numerical investigations in the current work are performed by using the CFD code LESOCC2 (Large-Eddy Simulation On Curvilinear Coordinates) which was developed for the simulation of complex turbulent flows. LESOCC2 is based on a cell centered 3D finite-volume method for block-structured grids. A central differences approach of second-order accuracy is applied for the spatial discretization of diffusive and convective fluxes. For periodic boundaries, a Fourier-Solver has been implemented as described by Fröhlich (2006). Time marching is achieved by applying a multi-stage low-storage, explicit Runge-Kutta method of second-order accuracy.

LESOCC2 solves the three-dimensional, unsteady, filtered and incompressible Navier-Stokes equations. Similar to statistically averaged equations, a closure problem arises so that different sub-grid-scale models are implemented in LESOCC2 to solve this problem. In the present work, the Smagorinsky model (Smagorinsky, 1963) is applied with Van Driest damping near solid walls. It is an eddy-viscosity model to parameterize the sub-grid-scale stresses

$$\tau_{ij}^a = \tau_{ij} - \tau_{kk} \frac{1}{3} \delta_{ij} \quad (9)$$

where δ_{ij} is the Kronecker delta. The isotropic part of the sub-grid-scale stresses τ_{kk} is not modeled but added to the static pressure term using a "pseudo" pressure $\bar{\Pi} = \bar{p} + \tau_{kk}/3$ (Fröhlich, 2006). The rest is modeled using a dimensionless empirical parameter.

$$\tau_{ij} = -2\nu_{sgs} \bar{S}_{ij}; \bar{S}_{ij} = \frac{1}{2} \left(\frac{\partial \bar{u}_i}{\partial x_j} + \frac{\partial \bar{u}_j}{\partial x_i} \right). \quad (10)$$

The Smagorinsky viscosity ν_{sgs} is modeled with the width of the filter Δ and the shear-stress rate S , as shown in Eq. 11, with the Smagorinsky constant being set to $C_s = 0.065$ for channel flows.

$$\nu_{sgs} = (C_s \Delta)^2 \sqrt{2 \bar{S}_{ij} \bar{S}_{ij}} \quad (11)$$

For mass conservation, the SIMPLE algorithm with pressure-correction equation is solved using the strongly implicit method of Stone (1968). The velocity-pressure coupling is achieved by applying the momentum interpolation method of Rhie and Chow (1983). LESOCC2 is highly vectorized with a vectorization ratio >99 % and additionally parallelized via the domain decomposition technique with the use of ghost cells and MPI for data transfer.

Computational domain and mesh

The computational domain in the current work, shown in Fig. 3, consists of a channel with the dimension $8.68\delta \times 2\delta \times 8.68\delta$ in the x-, y- and z-direction. The main flow is always directed in a positive x-direction. Cyclic boundary conditions are applied to the inlet and outlet as well as to the domain boundaries in z-direction, so that a channel of infinite dimensions in x- and z-direction is simulated. The upper wall of the channel is always kept smooth whereas surface roughness is applied to the lower wall. A block structured mesh with 64 blocks is used for spatial discretization. Details of the computational grid are listed in Tab. 1. The Reynolds number of all simulations is set to $Re = 13750$, which leads to an $Re_\tau = 395$ for a channel flow with smooth walls. In LESOCC2 computations are carried out with non-dimensional parameters. The density is set to $\rho = 1$ and the bulk-velocity to $U_b = 1$.

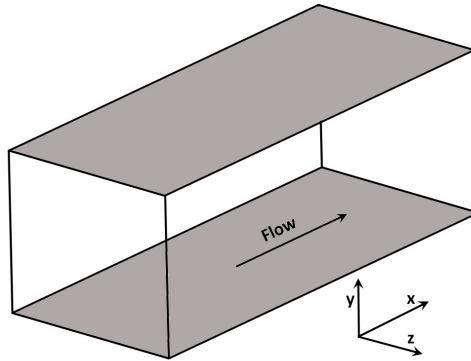


Figure 3: **Computational domain**

The roughness of the bottom wall is derived from surface roughness measurements. The anisotropic part of the surface roughness is the subject of the current study. To build a realistic model of it, the isotropic and anisotropic parts of measured surfaces have to be separated. On the left side of Fig. 4 and Fig. 5 the measured turbine surface roughness are shown. To build a surface model, a Fast-Fourier-Transformation (FFT) is used to isolate the 50 most dominant frequencies, which capture all

Roughness Type	A	B
Domain length	x=4.3 y=1 z=4.3	
$N_x \times N_y \times N_z$	315x221x192	192x221x315
Total number of cells	≈ 12.7 Mio	
Grid width	$\Delta x_c^+ \approx 10$	$\Delta x_c^+ \approx 18$
	$\Delta y_w^+ \approx 1$	$\Delta y_w^+ \approx 1$
	$\Delta y_c^+ \approx 10$	$\Delta y_c^+ \approx 10$
	$\Delta z_c^+ \approx 18$	$\Delta z_c^+ \approx 10$
Growth ratio	in y-direction: 3%, in x-,z-direction: uniform	

Table 1: **Details of computational grid employed**

of the relevant anisotropic structures. By setting all other frequencies to zero and doing an inverse transformation, the roughness models are obtained, as shown on the right side in Fig. 4 and Fig. 5. The topology of the roughness types A and B in Tab. 1 are the same, but with different flow directions. The main flow direction of the roughness A is perpendicular to the grooves whereas the grooves of roughness B are aligned parallel to the main flow direction.

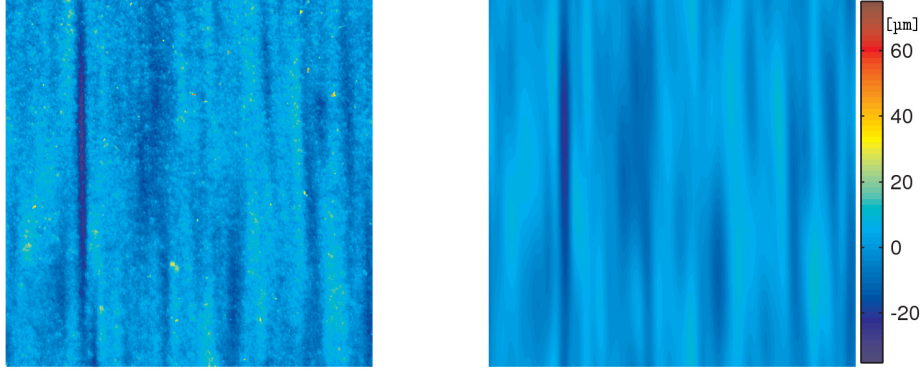


Figure 4: **Real and model roughness type A**

A scaling of the surface models is necessary due to the non-dimensionality of LESOCC2. The parameter used for scaling is the dimensionless arithmetic roughness height Ra^+ , defined in Eq. 12. It is the arithmetic roughness height made dimensionless with the friction velocity u_τ of the smooth wall and the kinematic viscosity ν .

$$Ra^+ = \left(\frac{1}{l} \sum_{i=1}^N |h(x_i)| \right) \cdot u_\tau / \nu \quad (12)$$

The measured roughness topology is stored in a matrix. Ra is determined for each row of the matrix and finally averaged over the number of rows. For the roughness of type A and B, the dimensionless arithmetic roughness heights are set to $Ra^+ = 5.76$. These values are chosen because they correspond to the Ra^+ of the turbine blade.

Numerical Accuracy

The methods and grids employed in a LES have a first order impact on the accuracy of the results, because the filter width $\bar{\Delta}$, which is used to calculate the sub-grid-scale viscosity ν_{sgs} , is a function of the mesh distances Δx_i . Therefore the sub-grid model is an explicit function of the grid. In order to

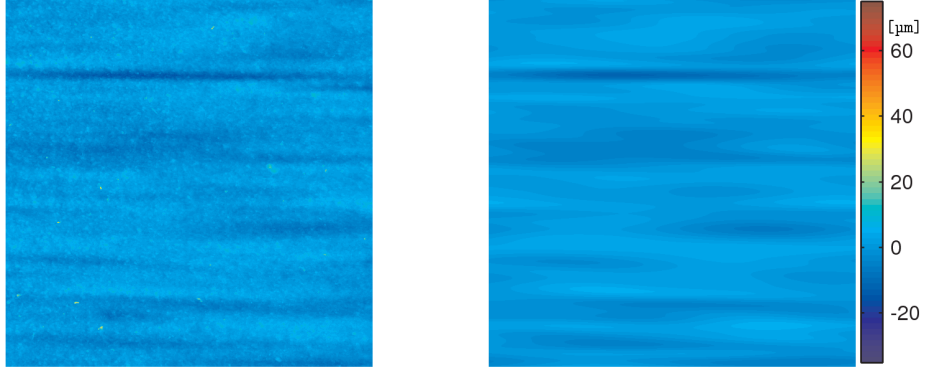
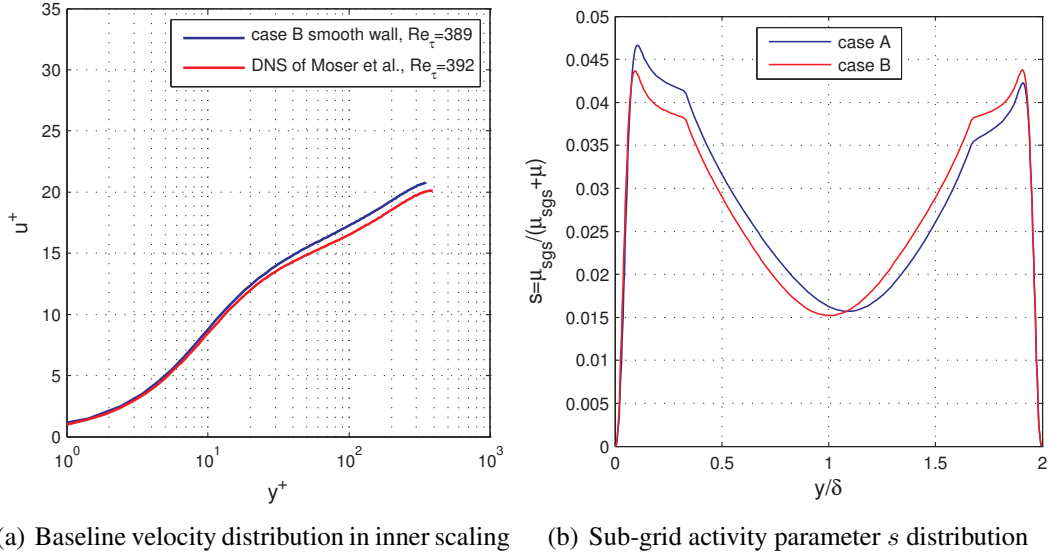


Figure 5: Real and model roughness type B



(a) Baseline velocity distribution in inner scaling (b) Sub-grid activity parameter s distribution

Figure 6: Verification of grid and methods employed

check the accuracy of the simulations carried out, the velocity distribution of the smooth wall of case B is compared with the results of Moser et al. (1999) which is shown in Fig. 6. It can be seen, that the velocity is slightly overpredicted for $y^+ > 20$ which is caused by the application of sub-grid stress modeling and has also been reported by Cui et al. (2003b). The deviation of the velocity distribution is well within the range reported by Cui et al. (2003b).

The sub-grid activity parameter s defined by Durbin and Pettersson-Reif (2011) as the ratio of sub-grid viscosity to total viscosity

$$s = \frac{\mu_{sgs}}{\mu_{sgs} + \mu}. \quad (13)$$

For values of $s < 0.5$ the accuracy of the LES is high and within the range of a DNS. The distributions of the average sub-grid activity parameter s for the cases A and B along the channel height is given in Fig. 6. For both cases the sub-grid activity parameter is well below $s = 0.05$, which is one tenth of the requested value for high accuracy of Large-Eddy-Simulations. Therefore it can be concluded from Fig. 6 that grid resolution and quality is high enough for a good accuracy.

It is known that the Smagorinsky model has a weak point when applied to wall resolved LES. The model leads to an error because the Smagorinsky constant remains $C_s \neq 0$ in near wall regions where

the grid resolution is high enough for a DNS. Although this leads to an error, Peet et al. (2008) showed that the application of the Smagorinsky model for this kind of investigation is possible. They carried out different LES to investigate the drag reducing effect of Riblets using the classical Smagorinsky model among others. Their results with the classical Smagorinsky model were consistent with other numerical and experimental results.

In order to evaluate the average wall shear stress the averaging time has to be high. The non-dimensional computational time

$$t^+ = \frac{t \cdot U_b}{\delta} \quad (14)$$

is introduced as a function of the computational time t , the channel half height δ and the bulk velocity U_b . It has been shown by Peet et al. (2008) that the drag reduction R_D of Riblets shows fluctuations of $\pm 2\%$ for averaging times $t^+ < 800$. In the present study averaging has been carried out after a non-dimensional time of $t_A^+ = 1370$ for case A and $t_B^+ = 1854$ for case B.

RESULTS

The roughness element shape and density parameter Λ_s and the equivalent sand grain height of the different roughnesses are calculated using Eq. 8 and Eq. 6. Additionally the predicted values of the roughness function (Eq. 5) and those with LES simulated are calculated and listed in Tab. 2. For the roughness height k of Eq. 6 half of the averaged maximum height of the roughness profile Rz is chosen: $k = 0.5 \cdot Rz$.

$$Rz = \frac{1}{n} \sum_{i=1}^N (|h_{min}(x_i)| + |h_{max}(x_i)|) \quad (15)$$

Roughness Type	Λ_s	k_s	k_s^+	$\Delta u_{predicted}^+$	Δu_{LES}^+	$\tau_{w,smooth}$	$\tau_{w,rough}$
A	892.6	0.0087	6.67	1.48	1.38	0.0030	0.0031
B	$8.05 \cdot 10^5$	0	0	0	0	0.0032	0.0032

Table 2: Summary of results of the Large-Eddy-Simulations

Both Sigal and Danberg (1990) and van Rij et al. (2002) applied their correlations to calculate an equivalent sand grain height only to values of $\Lambda_s < 1000$. Additionally Bons et al. (2001) showed that a brand-new, smooth turbine blade has a value of $\Lambda_s = 5000$, so that in the present study surfaces with $\Lambda_s > 1000$ are assumed to be smooth.

For every time-step the wall shear stress of every surface node has been stored into a matrix. The wall shear stress is defined in terms of the wall normal velocity gradient and the total viscosity μ .

$$\tau_w = \mu \frac{\partial u}{\partial n} \quad (16)$$

The wall shear stress has been averaged over the dimensionless time as stated before and afterwards spatially averaged on the walls. The resulting wall shear stresses are listed in Tab. 2. The wall shear stress contains viscous stresses as well as the pressure drag of the roughness elements.

From the simulations a dimensionless roughness height of $k_s^+ = 6.67$ has been determined for roughness A, which is within the buffer layer and very close to hydraulically smooth. From this point of view the roughness function Eq. 5 is not applicable to the present case. On the other hand the effect of the roughness A on the flow is significant. The existence of a critical roughness height, below which roughness does not affect the turbulent wall flow, has been questioned by Bradshaw (2000). Furthermore, he pointed out some "confusion over the variation of the friction factor or log-law shift for so called *transitionally roughness*" (Bradshaw, 2000, pg.2). In these premises and the fact, that

the application of the roughness function gives good results, it is assumed that the application of the roughness function in the present study is valid.

The mean velocity profiles in inner scaling for the smooth top walls and the different roughnesses of the bottom channel walls are shown in Fig. 7. The solid lines are the results of the Large-Eddy-Simulations whereas the diamonds are calculated using the equations Eq. 2 and Eq. 5. The effect of surface roughness is seen as a downward shift of the velocity u^+ for $y^+ > 70$ for the roughnesses A of the amount of $\Delta u^+ = 1.38$. In Fig. 7 (b), the velocity distribution for the rough surface B are found to be identical to those for the smooth wall .

To calculate the theoretical velocity distribution the commonly used values for the von Kármán constant $\kappa = 0.4$ and the integration constant $C^+ = 5.2$ are used for roughness B. For the rough surface A, the values have to be adapted. Although the upper channel wall is kept smooth in the LES, the influence of the bottom surface roughness is visible. Therefore the parameters κ and C^+ are adjusted to fit the smooth wall. These values are used further on to calculate the theoretical velocity distributions of the corresponding rough surfaces.

Mean velocity profiles in velocity defect form are shown in Fig. 8. Roughness B shows a very good agreement of the profiles of the smooth and rough wall over the whole boundary layer thickness. The results for roughness A show a deviation between the smooth and the rough wall profiles in the region $0.1 < y/\delta < 0.5$. As stated by Schultz and Flack (2005) a weak roughness effect results in a departure of the velocity profiles with the smooth wall profile lying above the rough wall profile and vice versa for a strong roughness influence. In the present study the rough wall profile is above the smooth wall profile in the buffer layer. This indicates a strong effect of the surface roughness. However, the velocity profiles collapse in the outer region for $y/\delta \geq 0.5$ which supports the wall similarity hypothesis of Townsend.

The skin friction, measured in terms of wall shear stress τ_w , was also evaluated for the two simulated surfaces. An increase of the wall shear stress $\Delta\tau_w$, compared to the smooth wall, can be observed for roughness A by $\Delta\tau_w = 3\%$. No change in wall shear stress was found for roughness B.

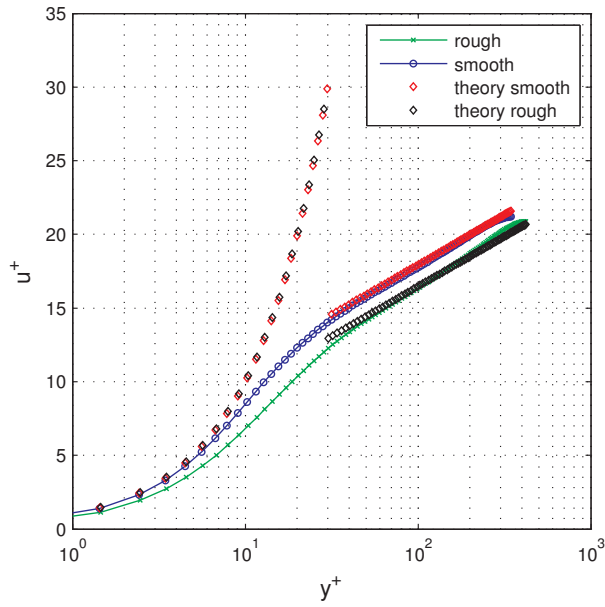
CONCLUSIONS AND OUTLOOK

The results of the present study show that the calculation of an equivalent sand grain roughness height is an appropriate way to predict the influence of inhomogeneous, anisotropic surface roughness which is close to reality. This is done using the roughness element shape and density parameter Λ_s of Sigal and Danberg (1990) and the correlation of Bons (2005) to estimate an equivalent sand grain height. As shown in Fig. 7 and in Tab. 2, the shift of the velocity profile Δu^+ is predicted sufficiently accurately. Only anisotropic surface roughness in which the main flow velocity vector has a component perpendicular to the anisotropy of the roughness affects the skin friction.

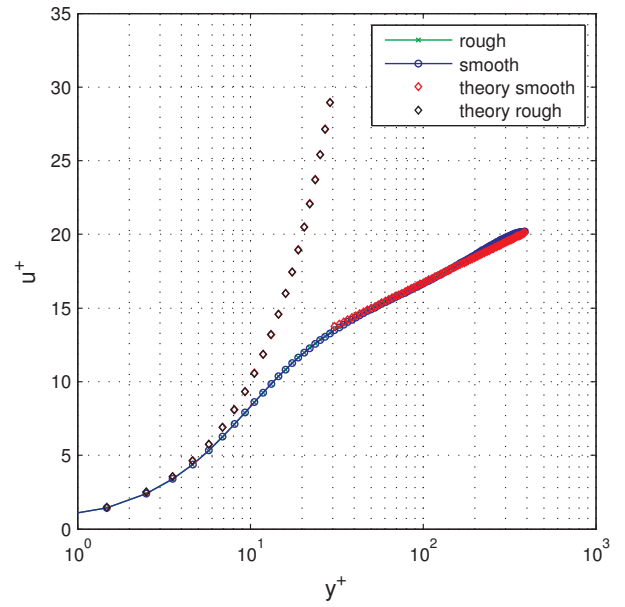
Additionally, the Reynolds number similarity hypothesis is confirmed by the results shown in Fig. 8. Differences in the velocity defect for roughness A are only visible in the inner layer. The velocity distributions in the outer layer match well in the rough and smooth cases. This result concurs well with previous studies of Lee et al. (2010), Kunkel et al. (2007) and Flack et al. (2005). In former investigations, LES was used to simulate the flow over homogenous anisotropic surface roughness such as ribs and sinusoidal waves. In the present study it could be shown that Large-Eddy-Simulations are also an appropriate method for predicting the influence of non-homogenous anisotropic surface roughness on the wall shear stress.

ACKNOWLEDGEMENTS

The authors kindly thank the German Research Foundation (DFG) for the financial support under grant SFB871/1 to accomplish the research project B3 "Influence of Complex Surface Structures on the Aerodynamic Losses of Turbomachinery Blades" within the framework of the Collaborative Research Centre (SFB) 871.

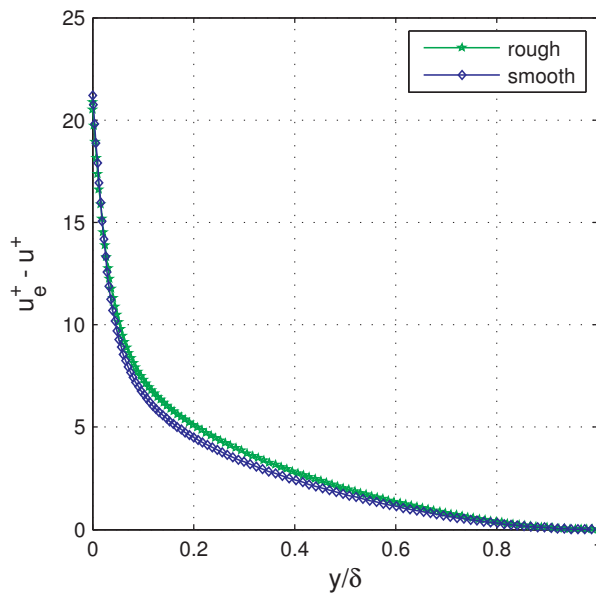


(a) Roughness A, $\kappa = 0.34$, $C^+ = 4.4$

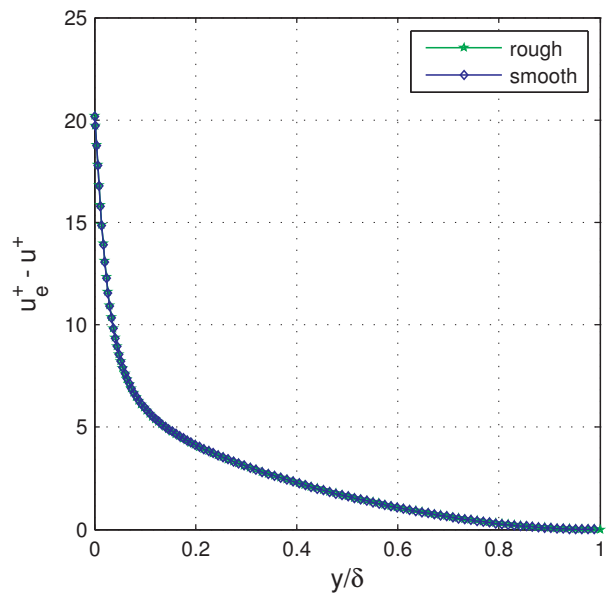


(b) Roughness B, $\kappa = 0.40$, $C^+ = 5.2$

Figure 7: Mean velocity profiles in inner scaling



(a) Roughness A



(b) Roughness B

Figure 8: Mean velocity profiles in form of velocity defect

REFERENCES

- Achary, M., Bornstein, J., Escudier, M. P., 1986. Turbulent boundary layers on rough surfaces. *Experiments in Fluids* (4), 33–47.
- Bons, J. P., 2002. St and cf Augmentation for Real Turbine Roughness With Elevated Freestream Turbulence. *Transactions of the ASME* (124), 632–644.
- Bons, J. P., 2005. A Critical Assessment of Reynolds Analogy for Turbine Flows. *ASME Journal of Heat Transfer* (127), 472–485.
- Bons, J. P., 2010. A Review of Surface Roughness Effects in Gas Turbines. *ASME Journal of Turbomachinery* (132).
- Bons, J. P., Taylor, R. P., McClain, S. T., Rivir, R. B., 2001. The Many Faces of Turbine Surface Roughness. *ASME Journal of Turbomachinery* (123), 739–748.
- Bradshaw, P., 2000. A note on “critical roughness height” and “transitional roughness”. *Physics of Fluids* 12 (6), 1611.
- Cai, X. M., Steyn, D. G., 1996. The von Karman constant determined by large eddy simulation. *Boundary-Layer Meteorology* 78, 143–164.
- Cui, J., Lin, C.-L., Patel, V. C., 2003a. Use of Large-Eddy-Simulation to Characterize Roughness Effect of Turbulent Flow Over a Wavy Wall. *Journal of Fluids Engineering* (125), 1075–1077.
- Cui, J., Patel, V. C., Lin, C.-L., 2003b. Large-eddy simulation of turbulent flow in a channel with rib roughness. *International Journal of Heat and Fluid Flow* 24 (3), 372–388.
- Durbin, P. A., Pettersson-Reif, B. A., 2011. *Statistical Theory and Modeling for Turbulent Flows; Second Edition, 2nd Edition*. Wiley, United Kingdom.
- Flack, K. A., Schultz, M. P., 2010. Review of Hydraulic Roughness Scales in the Fully Rough Regime. *Journal of Fluids Engineering* (132).
- Flack, K. A., Schultz, M. P., Shapiro, T. A., 2005. Experimental support for Townsend’s Reynolds number similarity hypothesis on rough walls. *Physics of Fluids* 17 (3), 035102.
- Frenzen, P., Vogel, C. A., 1995. On the magnitude and apparent range of variation of the von Karman constant in the atmospheric surface layer. *Boundary-Layer Meteorology* 72, 371–392.
- Fröhlich, J., 2006. *Large Eddy Simulation turbulenter Strömungen*. Teubner, Wiesbaden.
- Iacone, G. L., Reynolds, A. M., Tucker, P. G., 2008. Particle Deposition Onto Rough Surfaces. *Journal of Fluids Engineering* (130).
- Ikeda, T., Durbin, P. A., 2007. Direct simulations of a rough-wall channel flow. *Journal of Fluid Mechanics* (571), 235–263.
- Kunkel, G. J., Allen, J. J., Smits, A. J., 2007. Further support for Townsend’s Reynolds number similarity hypothesis in high Reynolds number rough-wall pipe flow. *Physics of Fluids* 19, 055109–1–055109–6.
- Lee, S.-H., Lee, J. H., Sung, H. J., 2010. Direct Numerical Simulation and PIV Measurement of Turbulent Boundary Layer over a Rod-Roughened Wall.

- Moser, R. D., Kim, J., Mansour, N. N., 1999. Direct numerical simulation of turbulent channel flow up to $Re=590$. *Journal of Fluids Engineering* 11 (4), 943–945.
- Nikuradse, J., 1933. Strömungsgesetze in rauhen Röhren. *VDI-Forschungsheft* 361 (361).
- Peet, Y., Sagaut, P., Charron, Y., 2008. Turbulent Drag Reduction using Sinusoidal Riblets with Triangular Cross-Section. *Proceedings of the 38th AIAA Fluid Dynamics Conference and Exhibit*.
- Rhie, C. M., Chow, W. L., 1983. Numerical Study of the Turbulent Flow Past an Airfoil with Trailing Edge Separation. *AIAA Journal* (Vol. 21, No. 11), 1525–1532.
- Schlichting, H., 1936. Experimental Investigation of the Problem of Surface Roughness. *Ingenieur-Archiv* 1 (3).
- Schlichting, H., Gersten, K., 2005. *Grenzschichttheorie*, 10th Edition. Springer, Berlin-Heidelberg.
- Schultz, M. P., Flack, K. A., 2005. Outer layer similarity in fully rough turbulent boundary layers. *Experiments in Fluids* 38 (3), 328–340.
- Schultz, M. P., Flack, K. A., 2007. The rough-wall turbulent boundary layer from the hydraulically smooth to the fully rough regime. *Journal of Fluid Mechanics* 580, 381–405.
- Sigal, A., Danberg, J. E., 1990. New Correlation of Roughness Density Effect on the Turbulent Boundary Layer. *AIAA Journal* (28), 554–556.
- Singh, K. M., Sandham, N. D., Williams, J. J. R., 2007. Numerical Simulation of Flow over a Rough Bed. *Journal of Hydraulic Engineering* (133), 386–398.
- Smagorinsky, J., 1963. General Circulation Experiments with the Primitive Equations. *Monthly Weather Review* 91 (3), 99–164.
- Stone, H., 1968. Iterative Solution of Implicit Approximations of Multidimensional Partial Differential Equations. *SIAM J. Numer. Anal.* (Vol. 5, No. 3).
- van Rij, J. A., Belnap, B. J., Ligrani, P. M., 2002. Analysis and Experiments on Three-Dimensional, Irregular Surface Roughness. *ASME Journal of Fluids Engineering* (124), 671–677.